Supplementary Material for:

Role of aldehyde chemistry and NO_x concentrations in secondary organic aerosol formation

A. W. H. Chan[1], M. N. Chan[2], J. D. Surratt[1], P. S. Chhabra[1], C. L. Loza[1], J. D. Crounse[1], L. D. Yee[2], R. C. Flagan[1,2], P. O. Wennberg[2,3], J. H. Seinfeld[1,2,*]

[1] Division of Chemistry and Chemical Engineering, California Institute of Technology, Pasadena, CA
[2] Division of Engineering and Applied Science, California Institute of Technology, Pasadena, CA
[3] Division of Geological and Planetary Sciences, California Institute of Technology, Pasadena, CA
[*] Corresponding author, email: seinfeld@caltech.edu

1 Negative Chemical Ionization Tandem Mass Spectrometry

Tandem mass spectrometry (MS/MS) in the negative mode of the chemical ionization mass spectrometer has been used in previous studies to separate isobaric compounds (Paulot et al., 2009; Surratt et al., 2010). Details of MS/MS operation are described in Paulot et al. (2009). In brief, the parent ions selected in the first quadrupole enter the second quadrupole, where a small flow of nitrogen is added until the pressure reaches 2.5×10^{-3} hPa. Selected parent ions undergo collision-induced dissociation (CID), and the parent ions of isobaric compounds can exhibit different CID patterns and yield different fragment (daughter) ions. Hence, with the third quadrupole acting as a second mass filter for the daughter ions, this allows for separate measurement of these isobaric compounds. For example, first-generation hydroxy-hydroperoxide and second generation epoxydiol from isoprene low-NO_x photooxidation both have a molecular weight of 118, and are detected as cluster ions at m/z 203. The hydroxy-hydroperoxide, known as ISOPOOH, has a significant yield of the daughter ion m/z 63, most likely FCO_2^-, while the epoxydiol, known as IEPOX, is detected at daughter m/z 183, representing a neutral loss of HF from the cluster ion. The individual contribution to the parent ion signal can therefore be separated based on known daughter ions (Paulot et al., 2009).

In the MBO231 and MBO232 experiments, both dihydroxynitrate and hydroxy-PAN are formed during high-NO_x photooxidation. Both compounds have molecular weights of 165, and are detected as the cluster ion at m/z 250. During MBO231 photooxidation, significant daughter ion signals are observed at m/z's 62, 184 and 230. Both daughter m/z 184 and 230 are formed promptly and the time trends of their signals correlate very well with each other, and likely arise from the same compound. Their signals reach a maximum after 60 minutes of irradiation, and decrease rapidly until the OH precursor is depleted (see Fig. 16 in main text). In all experiments, more OH precursor was injected after 300 minutes of irradiation. Upon further addition of OH precursor, the ion signals at daughter m/z's 184 and 230 drop by more than 40%. The time trends are consistent with the first-generation C_5-dihydroxynitrate, formed from RO_2 + NO. The CID likely proceeds via the following reactions, resulting in neutral losses of HF and CF_2O to form daughter m/z's 230 and 184, respectively:

$$\begin{aligned} \mathrm{R \cdot CF_3O^- + M} &\rightarrow \mathrm{CF_2O \cdot R^-_{-H}\ (m/z\ 230) + HF + M} \\ \mathrm{R \cdot CF_3O^- + M} &\rightarrow \mathrm{HF \cdot R^-_{-H}\ (m/z\ 184) + CF_2O + M} \end{aligned}$$

Negative m/z 230 and 184 were also observed in the single MS mode, under both high-NO and high-NO_2 conditions (observed in this work and in Chan et al. (2009)), suggesting that the fragmentation can also occur without induced collisions in the second quadrupole.

The daughter ion at m/z 62 displayed a distinctly different time trend: the signal increased monotonically until the OH precursor was depleted. In high-NO photooxidation of MBO231, upon further addition of HONO, the signal of daughter m/z 62 increased slightly. This is characteristic of a second-generation product formed later in the reaction mechanism. In MBO231 photooxidation, the signal of m/z 62 was significantly lower in high-NO experiments than in high-NO_2 experiments, and was insignficant in MBO232 photooxidation. These observations are all consistent with m/z 62 being a characteristic daughter ion for the second-generation C_4-hydroxy-PAN, as formation of PAN is favored by high NO_2/NO ratio. It is likely that the weak PAN functional group fragments to form NO_3^- ion (m/z 62), but the fragmentation pathway is currently unclear.

References

Chan, A. W. H., Galloway, M. M., Kwan, A. J., Chhabra, P. S., Keutsch, F. N., Wennberg, P. O., Flagan, R. C., and Seinfeld, J. H.: Photooxidation of 2-methyl-3-buten-2-ol (MBO) as a potential source of secondary organic aerosol, Environ. Sci. Technol., 43, 4647–4652, 2009.

Paulot, F., Crounse, J. D., Kjaergaard, H. G., Kurten, A., St Clair, J. M., Seinfeld, J. H., and Wennberg, P. O.: Unexpected epoxide formation in the gas-phase photooxidation of isoprene, Science, 325, 730–733, 2009.

Surratt, J. D., Chan, A. W. H., Eddingsaas, N. C., Chan, M. N., Loza, C. L., Kwan, A. J., Hersey, S. P., Flagan, R. C., Wennberg, P. O., and Seinfeld, J. H.: Reactive intermediates revealed in secondary organic aerosol formation from isoprene, Proc. Natl. Acad. Sci. USA, in press, doi:10.1073/pnas.0911114107, 2010.

2 Chemical Composition of SOA from Unsaturated Aldehydes

Table S1: SOA constituents detected by UPLC/(–)ESI-TOFMS and AMS in acrolein/high-NO_2 experiments.

	[M – H]$^-$ [a]	UPLC/ESI-TOFMS Measured Mass	TOFMS Suggested Ion Formula	Error (mDa)	i-Fit	# of Acid Monomer Units (*n*)	Structure	[M – OH]$^+$ [b]	AMS Suggested Ion Formula [c]
Oligoester Series 1	105	105.0199	$C_3H_5O_4^-$	1.1	2.1	1	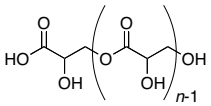	89	$C_3H_5O_3^+$
	193	193.0341	$C_6H_9O_7^-$	-0.7	3.9	2		177	$C_6H_9O_6^+$
	281	281.0493	$C_9H_{13}O_{10}^-$	-1.6	42.9	3		[d]	--
	369	369.0697	$C_{12}H_{17}O_{13}^-$	2.8	8.5	4		[d]	--
	457	457.0860	$C_{15}H_{21}O_{16}^-$	3.0	95.9	5		[d]	--
Oligoester Series 2	238	238.0172	$C_6H_8NO_9^-$	-2.7	8.7	1	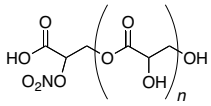	[d]	--
	326	326.0359	$C_9H_{12}NO_{12}^-$	1.6	23.8	2		[d]	--
	414	414.0539	$C_{12}H_{16}NO_{15}^-$	1.9	51.7	3		[d]	--
	502	502.0673	$C_{15}H_{20}NO_{18}^-$	-0.7	8.8	4		[d]	--
	590	590.0826	$C_{18}H_{24}NO_{21}^-$	-1.5	21.4	5		[d]	--
	678	678.1011	$C_{21}H_{28}NO_{24}^-$	1.0	12.1	6		[d]	--
	766	766.1182	$C_{24}H_{32}NO_{27}^-$	-3.8	16.7	7		[d]	--
	854	854.1367	$C_{27}H_{36}NO_{30}^-$	4.5	7.9	8		[d]	--
Oligoester Series 3 [e]	133	133.0142	$C_4H_5O_5^-$	0.5	5.4	1	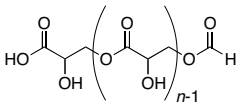	117	$C_4H_5O_4^+$
	221	221.0283	$C_7H_9O_8^-$	-1.4	30.1	2		[d]	--
	309	309.0453	$C_{10}H_{13}O_{11}^-$	-1.9	0.1	3		[d]	--
	397	397.0617	$C_{13}H_{17}O_{14}^-$	-0.1	11.4	4		[d]	--
	485	485.0775	$C_{16}H_{21}O_{17}^-$	-0.4	55.5	5		[d]	--
Oligoester Series 4 [f]	147	147.0313	$C_5H_7O_5^-$	-0.9	2.3	1	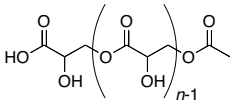	131	$C_5H_7O_4^+$
	235	235.0457	$C_8H_{11}O_8^-$	-0.7	1.8	2		219	$C_8H_{11}O_7^+$
	323	323.0627	$C_{11}H_{15}O_{11}^-$	1.3	14.4	3		[d]	--
	411	411.0823	$C_{14}H_{19}O_{14}^-$	4.8	12.6	4		[d]	--
	499	499.0945	$C_{17}H_{23}O_{17}^-$	1.0	42.9	5		[d]	--
	587	587.1115	$C_{20}H_{27}O_{20}^-$	1.9	2.1	6		[d]	--
	675	675.1276	$C_{23}H_{31}O_{23}^-$	2.0	4.0	7		[d]	--
	763	763.1435	$C_{26}H_{35}O_{26}^-$	1.8	2.3	8		[d]	--
	851	851.1621	$C_{29}H_{39}O_{29}^-$	4.4	6.4	9		[d]	--
Oligoester Series 5	283	283.0031	$C_6H_7N_2O_{11}^-$	-1.9	12.2	n/a	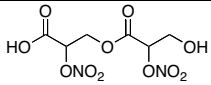	[d]	--

[a] Observed by UPLC/(-)ESI-TOFMS

[b] Observed by AMS V mode

[c] Suggested by AMS high-resolution W mode

[d] Not observed by AMS, most likely due to fragmentation of nitrate group, or below detection limit

[e] This oligoester series involves the esterification with formic acid.

[f] This oligoester series involves the esterification with acetic acid.

Table S2: SOA constituents detected by UPLC/(–)ESI-TOFMS and AMS in crotonaldehyde/high-NO_2 experiments.

	$[M-H]^-$ [a]	UPLC/ESI-TOFMS Measured Mass	TOFMS Suggested Ion Formula	Error (mDa)	i-Fit	# of Acid Monomer Units (*n*)	Structure	$[M-OH]^+$ [b]	AMS Suggested Ion Formula [c]
Oligoester Series 1	119	119.0342	$C_4H_7O_4^-$	-0.2	1.7	1	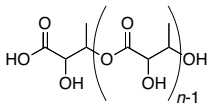	103	$C_4H_7O_3^+$
	221	221.0657	$C_8H_{13}O_7^-$	-0.4	18.6	2		205	$C_8H_{13}O_6^+$
Oligoester Series 2	266	266.0484	$C_8H_{12}NO_9^-$	1.3	22.5	1	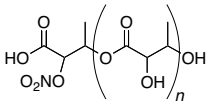	[d]	--
	368	368.0819	$C_{12}H_{18}NO_{12}^-$	-1.0	30.3	2		[d]	--
	470	470.1104	$C_{16}H_{24}NO_{15}^-$	-3.4	34.9	3		[d]	--
	572	572.1486	$C_{20}H_{30}NO_{18}^-$	2.3	5.1	4		[d]	--
	674	674.1761	$C_{24}H_{36}NO_{21}^-$	-1.9	10.7	5		[d]	--
	776	776.2100	$C_{28}H_{42}O_{24}^-$	0.3	10.6	6		[d]	--
	878	878.2444	$C_{32}O_{48}NO_{27}^-$	3.0	12.1	7		[d]	--
Oligoester Series 3 [e]	not detected					1	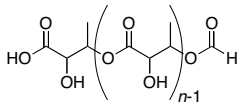	131	$C_5H_7O_4^+$
	249	249.06	$C_9H_{13}O_8^-$	-1.0	1.4	2		233	$C_9H_{13}O_7^+$
	351	351.0937	$C_{13}H_{19}O_{11}^-$	1.3	1.4	3		[d]	--
	453	453.1255	$C_{17}H_{25}O_{14}^-$	1.1	2.6	4		[d]	--
	555	555.1592	$C_{21}H_{31}O_{17}^-$	3.1	1.5	5		[d]	--
	657	657.1909	$C_{25}H_{37}O_{20}^-$	3.1	0.6	6		[d]	--
Oligoester Series 4 [f]	161	161.0461	$C_6H_9O_5^-$	0.4	2.2	1	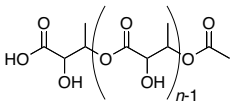	145	$C_6H_9O_4^+$
	263	263.0754	$C_{10}H_{15}O_8^-$	-2.1	7.5	2		[d]	--
	365	365.1087	$C_{14}H_{21}O_{11}^-$	1.5	15	3		[d]	--
	467	467.1401	$C_{18}H_{27}O_{14}^-$	-4.1	5.7	4		[d]	--
	569	569.1672	$C_{22}H_{33}O_{17}^-$	-4.6	20.6	5		[d]	--
	671	671.2040	$C_{26}H_{39}O_{20}^-$	0.5	0.6	6		[d]	--
Oligoester Series 5	not detected								

[a] Observed by UPLC/(-)ESI-TOFMS

[b] Observed by AMS V mode

[c] Suggested by AMS high-resolution W mode

[d] Not observed by AMS, most likely due to fragmentation of nitrate group, or below detection limit

[e] This oligoester series involves the esterification with formic acid.

[f] This oligoester series involves the esterification with acetic acid.

Table S3: SOA constituents detected by UPLC/(–)ESI-TOFMS in 2M2B/high-NO_2 experiments.

	[M – H]$^-$	UPLC/ESI-TOFMS Measured Mass	TOFMS Suggested Ion Formula	Error (mDa)	i-Fit	# of Acid Monomer Units (*n*)	Structure
Oligoester Series 1	133	133.0509	$C_5H_9O_4^-$	0.8	11.5	1	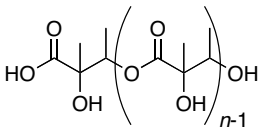
	249	249.0983	$C_{10}H_{17}O_7^-$	0.6	18.0	2	
	365	365.1466	$C_{15}H_{25}O_{10}^-$	1.8	16.3	3	
	481	481.1909	$C_{20}H_{33}O_{13}^-$	-1.2	64.5	4	
Oligoester Series 2	294	294.0819	$C_{10}H_{16}NO_9^-$	-0.6	90.8	1	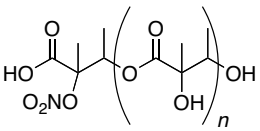
	410	410.1299	$C_{15}H_{24}NO_{12}^-$	-3.8	12.2	2	
	526	526.1761	$C_{20}H_{32}NO_{15}^-$	-1.1	3.2	3	
	641	642.2224	$C_{25}H_{40}NO_{18}^-$	-2.1	27.0	4	
Oligoester Series 3[a]	not detected					1	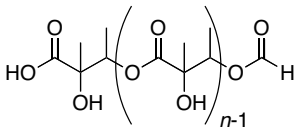
	277	277.0919	$C_{11}H_{17}O_8^-$	-0.4	20.5	2	
	393	393.1385	$C_{16}H_{27}O_{11}^-$	-1.2	25.8	3	
	509	509.1856	$C_{21}H_{33}O_{14}^-$	-1.4	3.1	4	
Oligoester Series 4[b]	not detected					1	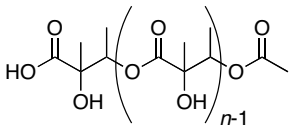
	291	291.1083	$C_{12}H_{19}O_8^-$	0.3	56.5	2	
	407	407.1536	$C_{17}H_{27}O_{11}^-$	-1.7	5.0	3	
	523	523.2034	$C_{22}H_{35}O_{14}^-$	0.7	18.1	4	
Oligoester Series 5	not detected						

[a] This oligoester series involves the esterification with formic acid.

[b] This oligoester series involves the esterification with acetic acid.

Table S4: SOA constituents detected by UPLC/(–)ESI-TOFMS in 2-pentenal/high-NO_2 experiments.

	$[M - H]^-$	UPLC/ESI-TOFMS Measured Mass	TOFMS Suggested Ion Formula	Error (mDa)	i-Fit	# of Acid Monomer Units (*n*)	Structure
Oligoester Series 1	133	133.0499	$C_5H_9O_4^-$	-0.2	1.1	1	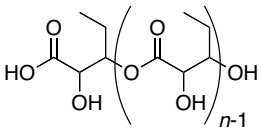
	249	249.0992	$C_{10}H_{17}O_7^-$	1.8	12.7	2	
	365	365.1447	$C_{15}H_{25}O_{10}^-$	-0.1	9.4	3	
Oligoester Series 2	294	294.0839	$C_{10}H_{16}NO_9^-$	1.4	5.2	1	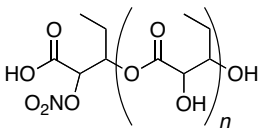
	410	410.1311	$C_{15}H_{24}NO_{12}^-$	1.2	1.9	2	
	526	526.1762	$C_{20}H_{32}NO_{15}^-$	-1.0	5.9	3	
	641	642.2251	$C_{25}H_{40}NO_{18}^-$	0.6	24.3	4	
Oligoester Series 3[a]		not detected				1	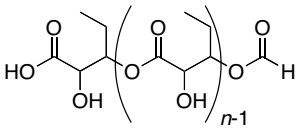
	277	277.0922	$C_{11}H_{17}O_8^-$	-0.1	12.5	2	
	393	393.1411	$C_{16}H_{27}O_{11}^-$	1.4	14.0	3	
Oligoester Series 4[b]		not detected				1	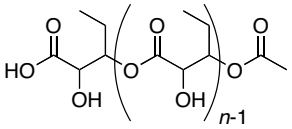
	291	291.1080	$C_{12}H_{19}O_8^-$	0.0	18.5	2	
	407	407.1555	$C_{17}H_{27}O_{11}^-$	0.2	10.5	3	
	523	523.2032	$C_{22}H_{35}O_{14}^-$	0.5	11.5	4	
Oligoester Series 5	not detected						

[a] This oligoester series involves the esterification with formic acid.

[b] This oligoester series involves the esterification with acetic acid.